SHALE ANISOTROPIC ELASTIC MODELING AND SEISMIC REFLECTIONS

XIAOYANG WU[1], RICHARD UDEN[2] and MARK CHAPMAN[3]

[1] *Edinburgh Anisotropy Project, British Geological Survey, Murchison House, West Mains Road, Edinburgh EH9 3LA, U.K. xywu@bgs.ac.uk*
[2] *Geoscience Consultant, Marathon Oil Corporation (retired), 5555 San Felipe, Houston, TX 77056, U.S.A.*
[3] *School of Geosciences, University of Edinburgh, The King's Buildings, West Mains Road, Edinburgh EH9 3JW, U.K.*

(Received February 15, 2016; revised version accepted September 25, 2016)

ABSTRACT

Wu, X., Uden, R. and Chapman, M., 2016. Shale anisotropic elastic modeling and seismic reflections. *Journal of Seismic Exploration*, 25: 527-542.

Shales are rocks with various mineralogy and complex fabric, which exhibit strong anisotropy. The change in effective velocities due to kerogen content and pore geometry influences the AVO (Amplitude Versus-Offset) behavior of shale-gas formations. How the conventional seismic survey plays its role in the exploration of unconventional shale gas is a key issue. In this paper, we present a method for estimating the anisotropic elastic stiffness of organic shales. The model takes mineralogy, kerogen, pore geometry and cracks, as well as the saturated fluids into consideration. A compaction-dependent Orientation Distribution Function (ODF) is incorporated to quantify the anisotropy originating from the preferential orientation of non-source shale inclusions. Comparison of the estimated elastic stiffnesses with experimental measurements of shale core sample from the Bazhenov formation indicates this method has the potential to estimate the elastic properties of organic shales. We also use another example from Eagle Ford formation to study the feasibility of distinguishing between proppant suspending hydraulic fluid and contacting with matrix during hydraulic stimulation stage. A half-space model with anisotropy due to multi-set of cracks is constructed to investigate the amplitude versus azimuthal and incident angle (AVAZ) reflections from the interface. The results indicate that the AVAZ behavior of PP reflection is different between proppant suspending fluid case and contacting with matrix case. The converted P-SH wave and SH-wave exploration may also offer detection of crack properties (distribution and intensity) to optimize shale gas production.

KEY WORDS: anisotropy, seismic reflection, hydraulic fracture, shale gas.

0963-0651/16/$5.00

INTRODUCTION

Organic shales as hydrocarbon source and reservoir rock are characterized by their strong anisotropy, which is one of current research subjects of shale gas formations. There are multiple causes of anisotropy in shales. First of all, clay platelets are the main constituent giving rise to strong anisotropy due to their shapes and preferential orientation during mechanical compaction and diagenesis. Organic richness can also have a significant influence on the anisotropy of shales. Vernik and Liu (1997) showed that matrix anisotropy of shales dramatically increases with kerogen reaching a moderate volume percentage. The presence of pores and micro-cracks at different stage of kerogen maturation is another reason for shale anisotropy. X-ray tomography showed that elongated cracks parallel to the shale bedding have been developed due to kerogen pyrolysis (Kobchenko et al., 2011; Allen et al., 2014). In

Understanding the anisotropic seismic response from different maturity of shales will improve our ability to characterize and predict 'sweet spots' from seismic data. Johansen et al. (2004) studied the P-P, P-SV, SV-SV and SH-SH reflections from the boundary separating an shale with VTI symmetry overlying an isotropic medium. The preferential orientation of shale platelets is characterized by the Gaussian ODF. However, more work still needs to be done on the anisotropic seismic response due to kerogen maturation, natural and induced cracks, fractures, and their application to field data. In this paper, we propose a method for estimating the anisotropic elastic stiffness of organic shales by combining existing rock physics models, in terms of shale constituents and fabric. It takes different mineralogy, kerogen, pores and fluids into account, aiming at analyzing the anisotropy of organic-rich shales quantitatively. A series of rock physics models are chosen to estimate the anisotropic elastic properties of a shale core sample from Bazhenov formation. We also propose a method to estimate the elastic properties and seismic AVAZ reflections for hydraulically fractured shales. The Hudson's model for cracked media that considers weak inclusions is used to model the fluid-proppant-matrix interaction. Numerical modeling is performed to understand the difference of using P-wave, SV-wave and SH-wave as incidence respectively. This method is applied to Eagle Ford shales before and after hydraulic stimulation.

METHOD

Anisotropic elastic modeling

In the procedure of estimating elastic properties of shales, selection of rock physics models are non-unique and depend on the knowledge of constituents and fabric. Shales contain a series of isotropic minerals like quartz, calcite, pyrite etc, and anisotropic constituents like clay with preferential orientation and bedding laminated kerogen, of which the latter make shales exhibit VTI symmetry. The Backus average can be used to estimate the elastic stiffness by considering two end members: organic matter and non-organic minerals. Bounds models such as the Voigt-Reuss-Hill average can be used to estimate the elastic moduli of non-organic minerals in terms of the volume percent of each mineral. An alternative choice is the inclusion models such as Differential Effective Medium (DEM) model, which incrementally adds inclusions of each phase to the matrix phase. For porous shales (e.g., Bazhenov, Monterey, Niobrara, etc.), the impact of pore structure and their saturated fluids on elastic properties needs to be taken into consideration. Combining DEM model with ODF can add pores and cracks with a particular preferential orientation. The saturated fluids in pores and cracks need to be considered by using the Brown and Korringa relations (1975) for low-frequency band.

The ODF plays an important role in quantifying the anisotropy caused by

preferred orientation of inclusions. ODF is a function of the three Euler angles θ, φ, ζ in 3D space, which can be expanded as a series of generalized spherical harmonic functions (Roe, 1965). For VTI symmetry, the ODF is only a function of θ. We can envisage the inclusion as transversely isotropic penny-shaped spheroid with semi-axes $\boldsymbol{a} < \mathbf{b} = \mathbf{c}$. Under such case, the elastic properties of the whole medium stay the same when rotating the spheroids an arbitrary angle around the original x3 (φ) and new x3′ (ζ) axes. Since the elastic tensor is fourth order tensor, the ODF only depends on W_{000}, W_{200} and W_{400}, of which W_{000} controls the isotropic part, while W_{200} and W_{400} control the transversely isotropic part of the ODF (Sayers, 1994; Johansen et al., 2004).

During shale gas production, Hudson's model (1980) for cracked media can be used to estimate the elastic properties of hydraulically fractured shales. A key issue when modeling hydraulically fractured shales is to consider the fluid-proppant saturation in the matrix. At early stage of hydraulic fluid injection, cracks are initiated or enlarged by high-pressure fluid, proppant suspends in the fluid, while at late stage when hydraulic fluid is recovered, proppant will hold fractures open and bridge fractures with matrix. Under such case, the shear modulus of fluid-proppant inclusions is considered by using Hudson's model (1981) for weak inclusions. We use Schoenberg and Protazio's (1992) explicit solution to the Zoeppritz equation for weakly anisotropic media to calculate reflectivities from the interface.

Anisotropic elastic modeling of the Bazhenov core sample

Vernik and Landis (1996) gave the average mineralogy (% vol.) of 8 shale core samples from the Bazhenov formation through Whole-Rock XRD Analysis. These core samples came from a single well located in the northeastern part of the West Siberian basin at depths from 3784 m to 3842 m. Vernik and Liu (1997) further provided the ultrasonic velocities of the 8 samples under dry condition and 5 samples under brine-saturated condition. Table 1 shows four mineral groups that dominate the mineralogy. The volume percentage of each mineral was given on a kerogen-free basis. We take the average mineralogy as an example, and assume that the volume percentage of kerogen is 16.8%, the porosity is 4.12% (referring to No. 3 sample of Bazhenov in Appendix A, Vernik and Liu, 1997). The elastic moduli of clay are cited from Hornby et al. (1994). The others are from Mavko et al. (1998). The elastic stiffness of dry rock and brine-saturated rock are estimated by combining different rock physics models.

First, we assume the non-organic shale and kerogen are intrinsically isotropic. Using the Voigt-Reuss-Hill average, we obtain the elastic moduli for non-organic shale are K = 32.08 GPa; μ = 23.92 GPa, corresponding to C_{33} = 63.97 GPa; C_{44} = 23.92 GPa; C_{12} = 16.13 GPa. According to the SEM

observation of Vernik and Landis (1996), kerogen forms the network and separates non-organic shale. We can add non-organic shales as the inclusions into kerogen content. Anisotropy is caused by the shape and preferential orientation of the inclusions. The anisotropic DEM model is used for the calculation of elastic tensor of kerogen and fully aligned non-organic shales composite. Fig. 1 displays four elastic stiffness curves changing with kerogen volume fraction by varying the aspect ratio of the inclusions. We can see that with increasing of aspect ratio, C_{11} and C_{44} become closer to C_{33} and C_{66}. Thinner inclusions exhibit higher anisotropy. When the aspect ratio is 1.0, C_{11} and C_{44} coincide with C_{33} and C_{66} respectively, exhibiting the characteristics of isotropy. Since the isotropic quartz/feldspar is almost as much as clay mineral

Table 1. The average volume percentage and elastic moduli for each constituent of the Bazhenov shale.

	quartz/ feldspar	carbonate	clay	Pyrite	kerogen	porosity	Fluid(brine)
% Vol	46	3	48	3	16.8	4.12	
K(GPa)	37	76.8	22.9	147.4	2.9		2.2
μ(GPa)	44	32	10.6	132.5	2.7		0

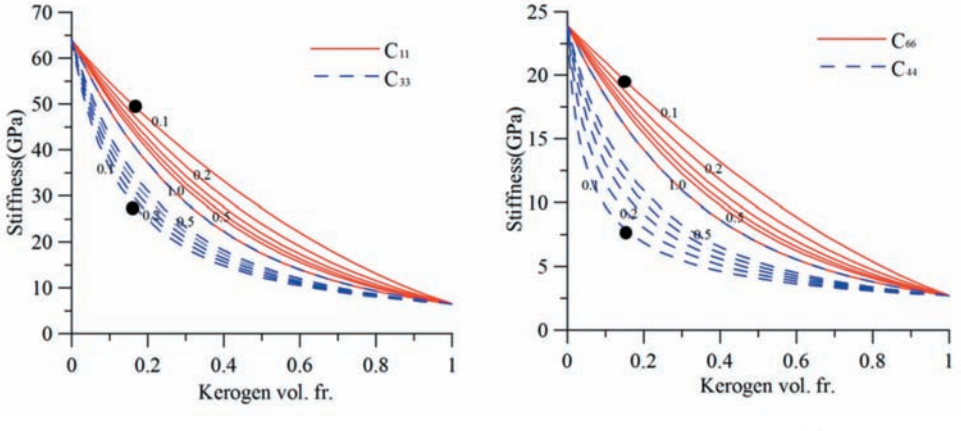

(a) C_{11} and C_{33} (b) C_{44} and C_{66}

Fig. 1. Stiffness changes with kerogen volume percent for the kerogen-shale using anisotropic DEM model. Kerogen background and shale inclusions are both considered to be isotropic. Shale aspect ratio = 0.1, 0.2, 0.3, 0.4, 0.5, 1.0.

in volume percent, we give an aspect ratio of 0.1 to calculate the stiffness of the kerogen-'shale' composite. The black spots correspond to the elastic tensors when kerogen volume percentage is 16.8%.

Fig. 2 displays the elastic stiffness when non-organic shale is fully aligned (solid lines) and partially aligned (dot lines) with a compaction factor c = 3.0. We can see the separation of C_{11} and C_{33}, C_{44} and C_{66} have been reduced, indicating the magnitude of anisotropy has been weakened after averaging on ODF. Black spots indicate the elastic stiffness when Kerogen volume fraction equal to 16.8%.

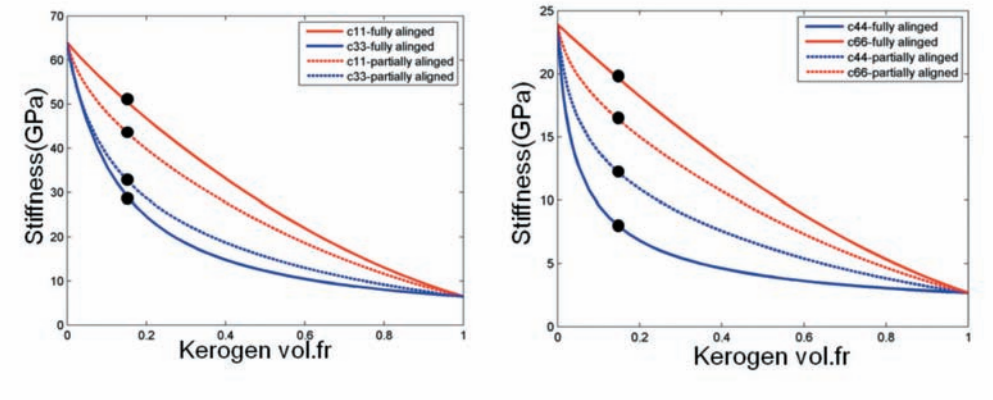

(a) C_{11} and C_{33} (b) C_{44} and C_{66}

Fig. 2. Elastic stiffness when shale is fully aligned (a) and partially aligned with a compaction factor c = 3.0. (b) Aspect ratio = 0.1.

Likewise, pores are added to the composite using the anisotropic DEM model again to form the dry rock. For simplicity, we give an average aspect ratio of 0.6 for the pores and assume the distribution of non-organic shale to be fully aligned. However, for the same porosity, pore types can cause different P-wave velocity. Xu and Payne (2009) considered different types of pores in their carbonate model. The bulk density of dry rock is 2.34 g/cm^3. The density of brine-saturated rock is 2.38 g/cm3. Fig. 3 displays the stiffness of dry rock changing with porosity. Evidently, stiffness decreases with increasing porosity.

Finally, the Brown-Korringa model is used to calculate the elastic stiffness for brine-saturated rock. Table 2 is a comparison of estimated stiffness and stiffness transformed from the measured velocities. We can see that the

predicted C_{33} increases more significantly after brine saturated under fully aligned case, but the predicted C_{44} and C_{66} remain the same when saturated with fluid. Anisotropy is weakened when shale inclusion is partially aligned. The error of C_{44} for the dry case is slightly larger than those of C_{11}, C_{33} and C_{66}. Fig. 4 displays the velocity and slowness when the shale inclusions are fully aligned (a) and partially aligned (b). We can see strong anisotropy for fully aligned case (a) and weak anisotropy for partially aligned (b) after averaging on ODF.

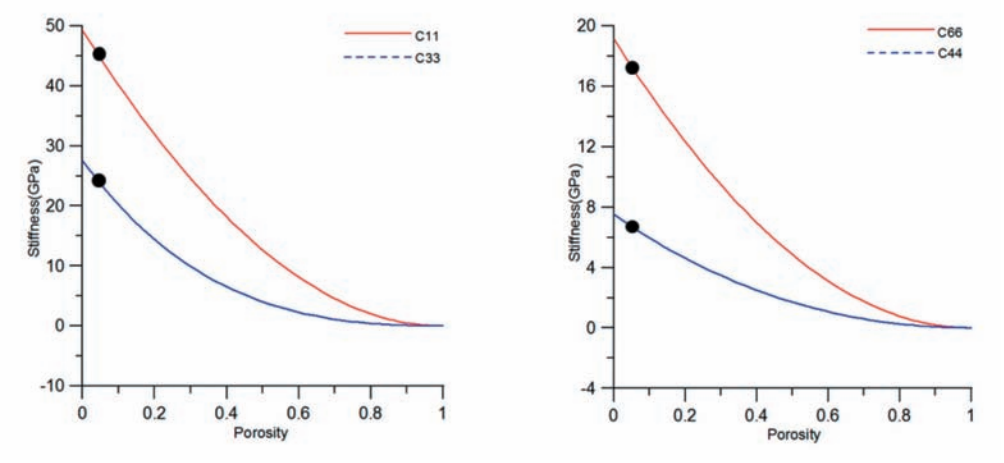

(a) C_{11} and C_{33} (b) C_{44} and C_{66}

Fig. 3. Elastic stiffness changes with porosity using anisotropic DEM model. Pore aspect ratio = 0.6.

Reflection modeling of hydraulic fractures for Eagle Ford shale

Table 3 displays the parameters of the model, of which the Eagle Ford shale parameters are referred to Yenugu (2015). An initial set of cracks with crack normal parallel to x1 direction is assumed to exist in both Austin Chalk and Eagle Ford shale respectively. The crack density and aspect ratio are 0.05 and 0.05 for Austin Chalk, 0.01 and 0.01 for Eagle Ford shale. Cracks are assumed to be saturated with fluid. We then assume two sets of cracks (one set with crack normal parallel to x1, the other set with crack normal parallel to x3) are introduced into Eagle Ford shale, which makes the medium become orthorhombic.

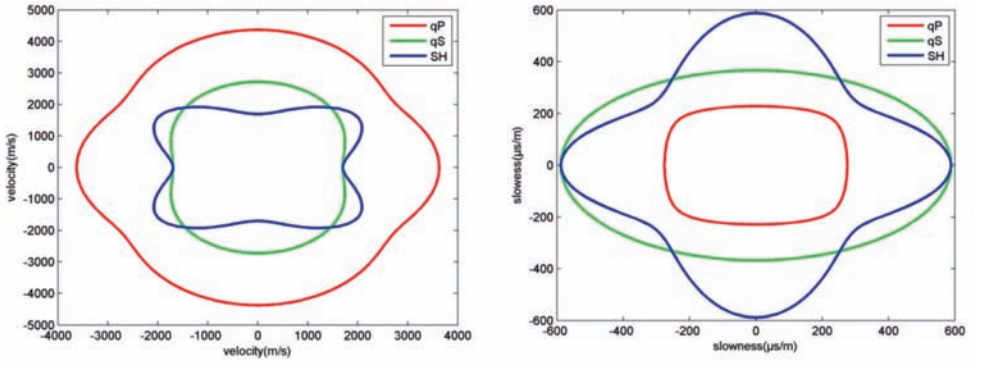

(a) The shale inclusions are fully aligned

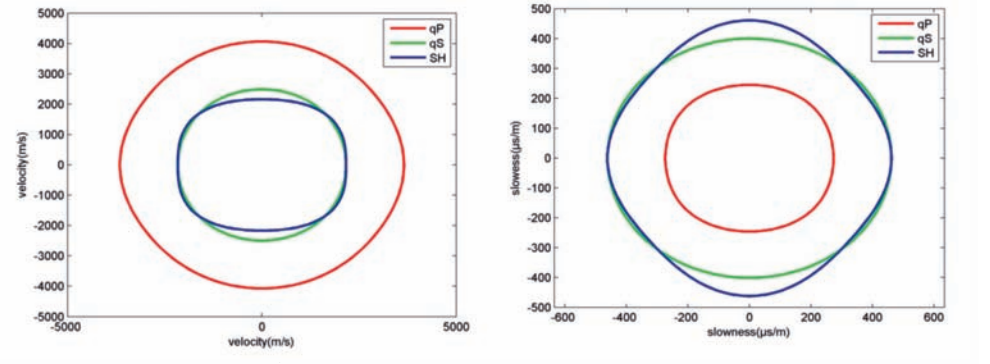

(b) The shale inclusions are partially aligned (a = 3.0)

Fig. 4. The modeled velocity and slowness assuming shale inclusions are fully aligned (a) and partially aligned with a = 3.0 (b).

Fig. 5 displays the fluid-proppant moduli varying with proppant volume for the two cases. Fig. 6 displays the Thomson parameters for the two cases. We can see ε, δ decreases when increasing proppant volume for both cases. For suspension case, shear anisotropy γ is considered to be constant. In the numerical modeling, we assume a 50% of proppant saturation in hydraulic fractures.

Fig. 7 displays the nine reflection coefficients varying with incident angle at 5 different azimuthal angles 0°, 30°, 45°, 60° and 90°, for the HTI-HTI model before hydraulic fracturing. The azimuthal dependence of P-P reflections

increases with incident angle. The amplitudes parallel to crack normal (90°) are expected to be higher than the amplitudes perpendicular to crack normal (0°) before 40° of incident angle. For converted P-SV reflection, amplitude magnitude increases with azimuthal angle, with no P-SV reflections at 0° and the strongest reflections at 90°, while the P-SH reflections show the reverse trend of variations from P-SV reflections. The azimuthal dependence of SV-SV and SH-SH reflections are significant. For SV-SH and SH-SV modes, no energy is reflected at 0° and 90° azimuthal angle. The strongest reflections occur at 45°.

Table 2. Comparison of predicted and measured elastic tensor for a shale sample from Bazhenov formation.

	Rock	C11 (GPa)	C33 (GPa)	C44 (GPa)	C66 (GPa)	C13 (GPa)
Predicted stiffness	Kerogen-'shale' (fully aligned)	49.25	27.60	7.53	19.11	7.01
	Dry (fully aligned)	45.44	24.43	6.87	17.62	6.35
	Brine-Saturated (fully aligned)	45.45	31.33	6.87	17.62	6.05
	Kerogen-'shale' (Partially aligned)	42.27	31.38	11.69	15.86	9.79
	Dry (Partially aligned)	38.85	28.35	10.69	14.58	8.91
	Brine-Saturated (Partially aligned)	39.42	31.80	10.69	14.58	9.14
Measured stiffness	Dry	45.50	25.17	10.32	17.82	
	Brine-Saturated	42.38	26.23	8.68	15.23	

Table 3. The parameters for the half-space model with Austin Chalk overlying Eagle Ford shales.

	lithology	V_{p0} (km/s)	V_{s0} (km/s)	ρ (g/cm^3)	anisotropy	α	ε
Upper	Austin Chalk	5.257	2.794	2.623	HTI	0.05(x1)	0.05(x1)
Lower	Eagle Ford shales	4.320	2.408	2.512	HTI (Pre-SRV)	0.01(x1)	0.01(x1)
					Orthorhombic (Post-SRV)	0.05(x1) 0.05(x3)	0.05(x1) 0.05(x3)

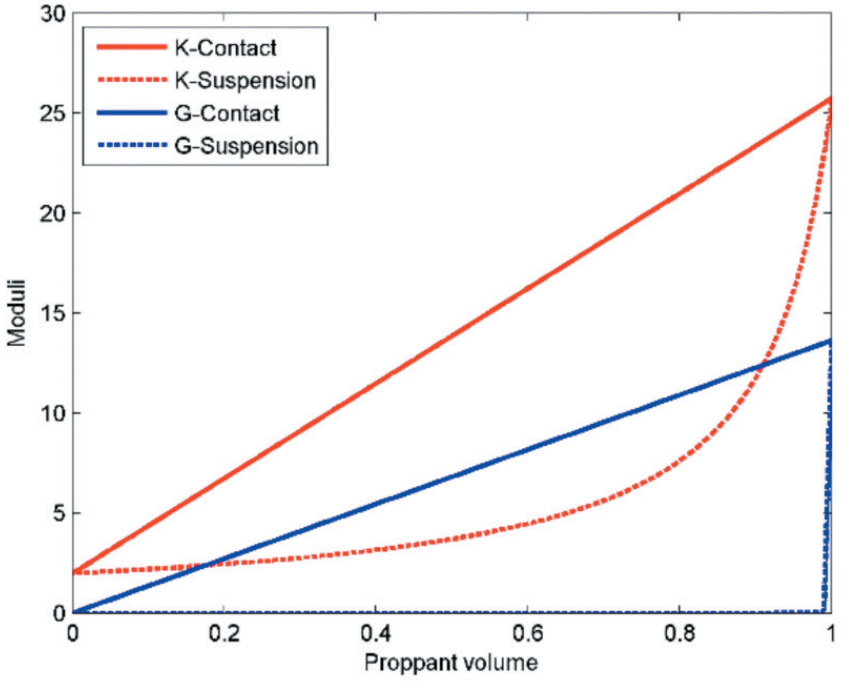

Fig. 5. Fluid-proppant moduli varying with volume of proppant for solid contact.

Fig. 8 displays the reflections after introducing two sets of cracks into Eagle Ford shale. The normals of the two sets of cracks are parallel to x1 and x3 respectively. proppant is considered to suspend in hydraulic fluid. A significant difference is the azimuthal PP reflections show a reverse behavior from Fig. 7 for Pre-SRV stimulation. We can also see the amplitudes magnitude for P-P, P-SH, SH-P, SH-SH reflections have increased due to the increasing impedance contrast between the lower and upper media.

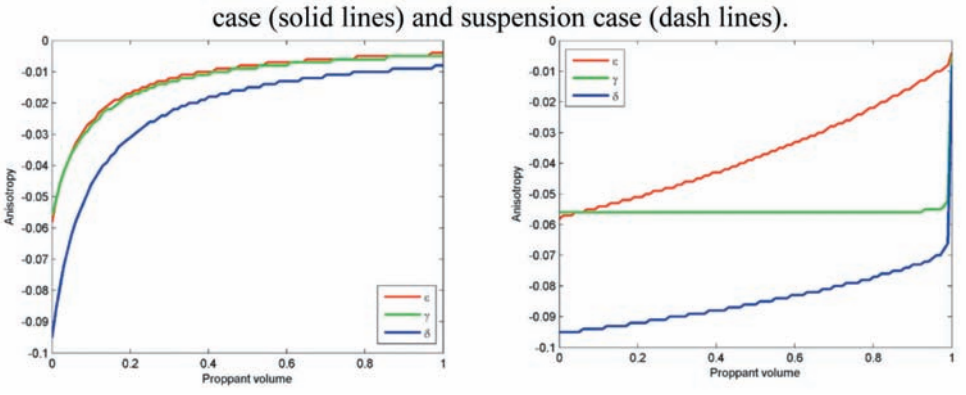

Fig. 6. Thomson parameters for solid contact case (left) and suspension case (right) - red = epsilon, green = gamma, blue = delta.

Fig. 9 displays the reflections when proppant contact with matrix. The characteristics of nine reflections are similar to Fig. 7 before SRV. A difference worth to mention is the azimuthal anisotropy of PP reflections have reduced. This indicates that it is possible to distinguish proppant suspending fluid from proppant contacting matrix by using seismic azimuthal PP reflections. The results of these reflections also give an important indication that the azimuthal SH-SH reflection magnitude and converted P-SH reflection magnitude are sensitive to cracks distribution. This indicates that the P-SH converted wave or SH wave as incidence may be used for the detection of crack distribution in the shale gas production. Fig. 10 displays the PP azimuthal AVO response for the above three rock physics models.

CONCLUSIONS

In this paper, we proposed a method for the anisotropic elastic modeling of organic shales. In terms of the constituents and fabric, different rock physics models are combined to estimate the elastic properties. The VTI symmetry of shales due to clay inclusions can be characterized by anisotropic DEM model. The aspect ratio and ODF are used to quantify the anisotropy originated from shapes and preferential orientation. Anisotropic DEM model can also be used to model pores and cracks with preferential orientations. This method turns out to be feasible when it is used to estimate the elastic stiffnesses of shale core sample from Bazhenov formation. When simulating hydraulic fracturing, Hudson's model for cracked media is suitable to estimate the elastic properties

of the medium with HTI and orthorhombic symmetry. We modelled the seismic AVAZ reflections with P, SV and SH wave mode as incidence. The results show that it may be feasible to distinguish proppant suspending fluid at early high fluid pressure stage from proppant contacting matrix at late lower fluid pressure stage. Azimuthal S-S reflections and converted P-SH reflections are sensitive to cracks distribution, which indicates that the converted wave and S-wave exploration may be effective for the detection of crack distribution during the stage of shale gas production.

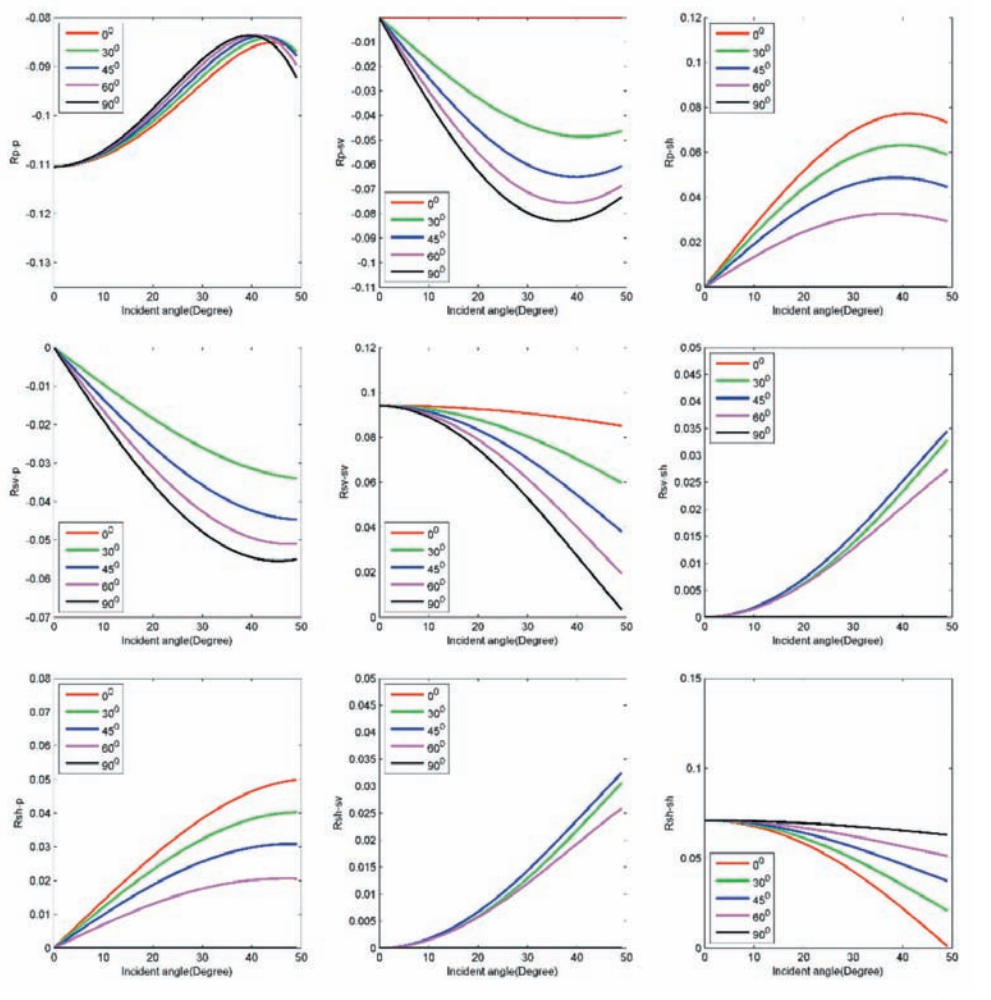

Fig. 7. Reflections from the interface of HTI-HTI model before SRV - red = 0°, green = 30°, blue = 45°, purple = 60°, black = 90° azimuth angles.

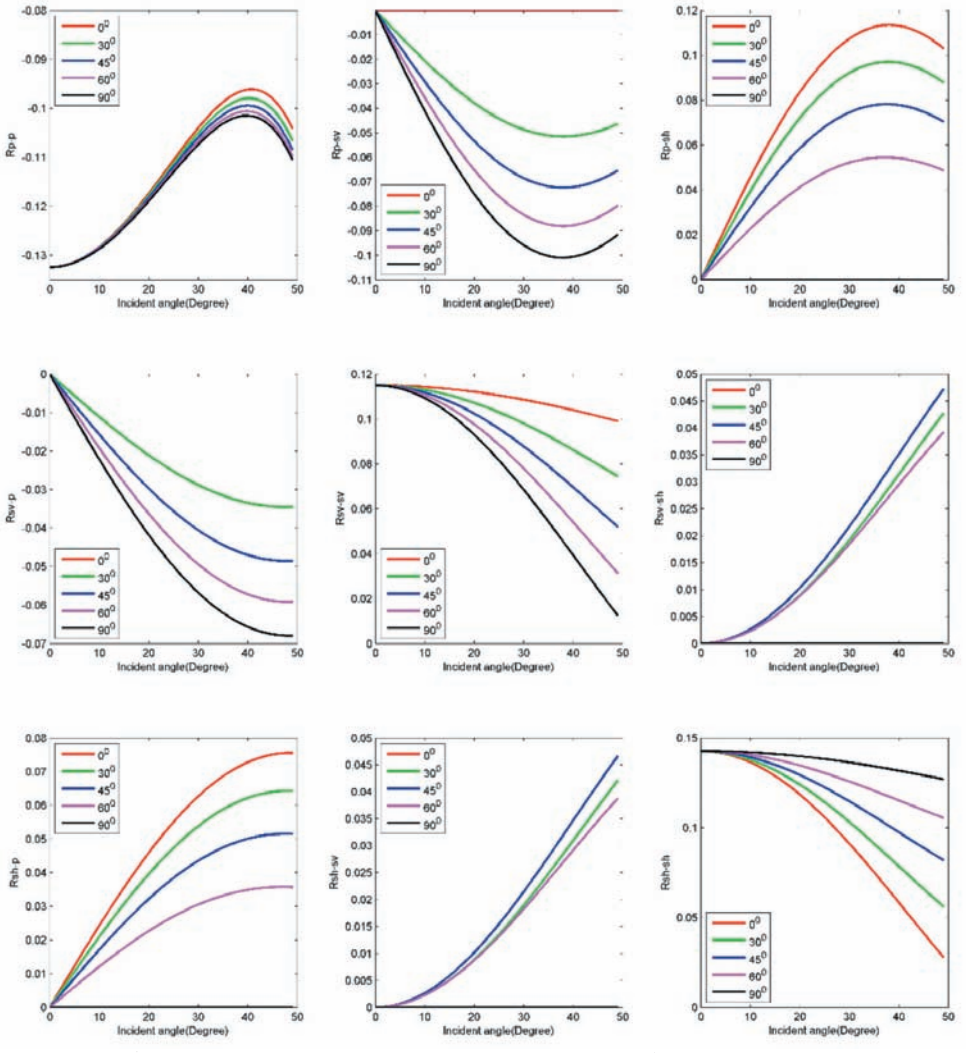

Fig. 8. Reflections from the interface of HTI-Orthorhombic model after SRV. Proppant is considered to be suspending in hydraulic fluid, and filled in fractures at early stage.

The model discussed here is one model approach that incorporates the shale complexities into the elastic descriptions for these anisotropic rocks. The ranges of response suggest that shear measurements are most sensitive to induced fractures as we might expect, while the propped versus unpropped conclusions would need to be validated by field measurements for example.

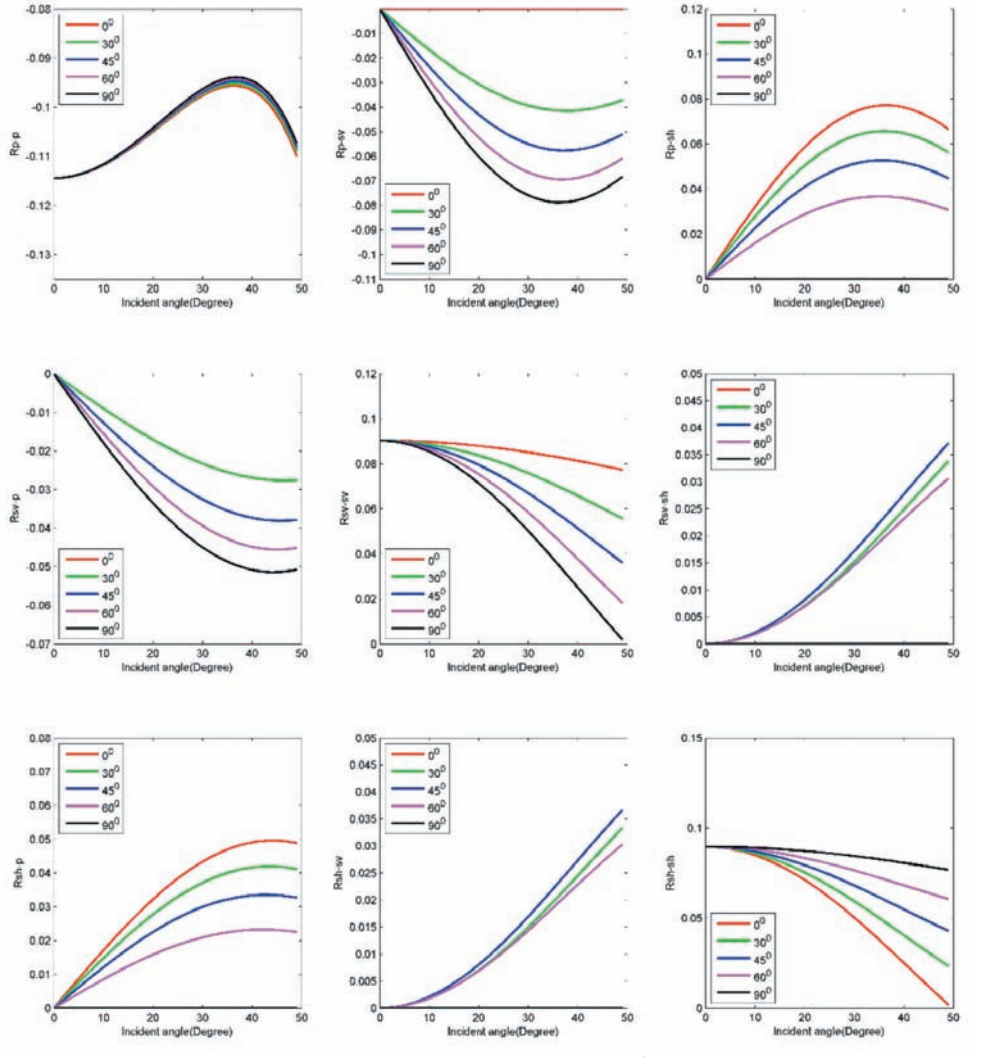

Fig. 9. Reflections from the interface of HTI - Orthorhombic model after SRV. Proppant is considered to bridge fractures and contact with matrix at late stage.

ACKNOWLEDGEMENTS

This work was supported by the sponsors of the Edinburgh Anisotropy Project (EAP), and is presented with the permission of the Executive Director of the British Geological Survey (Natural Environment Research Council).

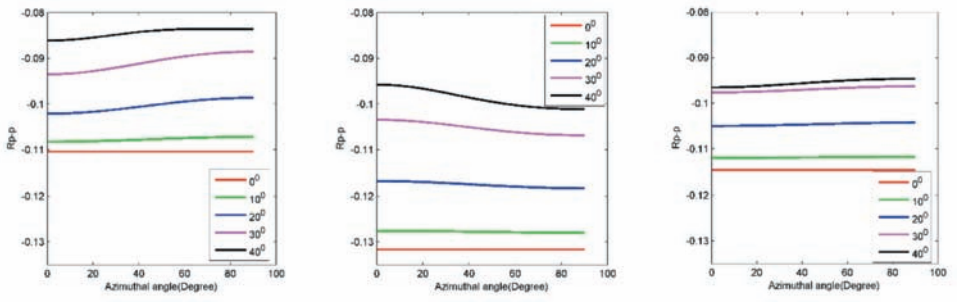

(a) HTI-HTI model

(b) HTI-Orthorhombic model when proppants suspension

(c) HTI-Orthorhombic model when proppants bridge fractures

Fig. 10. The PP Azimuthal AVO response at 5 incident angles 0°, 10°, 20°, 30°, 40° for (a) HTI-HTI model before hydraulic fracturing, (b) HTI-Orthorhombic model when proppants suspend in hydraulic fluid, and (c) HTI-Orthorhombic model when proppants contact the matrix.

REFERENCES

Allan, A.M., Vanorio, T. and Dahl, J.E., 2014. Pyrolysis-induced P-wave velocity anisotropy in organic rich shales. Geophysics, 79(2): D41-D53. doi: 10.1190/geo2013-0254.1

Bandyopadhyay, K., 2009. Seismic anisotropy-geological causes and its implications to reservoir geophysics. Ph.D. thesis, Stanford University, Stanford.

Brown, R. and Korringa, J., 1975. On the dependence of the elastic properties of a porous rock on the compressibility of the pore fluid. Geophysics, 40: 608-616. doi: 10.1190/1.1440551

Curtis, J.B., 2002. Fractured shale-gas systems. AAPG Bulletin, 86(11), 1921-1938. doi: 10.1306/61EEDDBE-173E-11D7-8645000102C1865D

Gale, J.F.W., Reed, R.M. and Holder, J., 2007. Natural fractures in the Barnett Shale and their importance for hydraulic fracture treatments. AAPG Bull., 91(4): 603-622. doi: 10.1306/11010606061

Hornby, B.E., Schwartz, L.M. and Hudson, A.J., 1994. Anisotropic effective-medium modeling of the elastic properties of shales. Geophysics, 59, 1570-1583. doi: 10.1190/1.1443546

Hudson, J.A., 1980. Overall properties of a cracked solid. Math. Proc. Camb. Phil.Soc., 88, 371-384. doi: 10.1017/S0305004100057674

Hudson, J.A., 1981. Wave speeds and attenuation of elastic waves in material containing cracks. Geophys. J. Roy. Astr. Soc., 64: 133-150. doi: 10.1111/j.1365-246X.1981.tb02662.x

Jakobsen, M., Hudson, J.A. and Johansen, T.A., 2003. T-matrix approach to shale acoustics. Geophys. J. Internat., 154: 533-558. doi: 10.1046/j.1365-246X.2003.01977.x

Johansen, T.A., Rudd, B.O. and Jakobsen, M., 2004. Effect of grain scale alignment on seismic anisotropy and reflectivity of shales. Geophys. Prosp., 52: 133-149. doi: 10.1046/j.1365-2478.2003.00405.x

Kobchenko, M., Panahi, H., Renard, F., Dysthe, D.K., Malthe-Sørenssen, A., Mazzini, A., Scheibert, J., Jamtveit, B. and Meakin, P., 2011. 4D imaging of fracturing in organic-rich shales during heating. J. Geophys. Res.: Solid Earth, 116: B12201. doi: 10.1029/2011JB008565

Mavko, G., Mukerji, T. and Dvorkin, J., 1998. The Rock Physics Handbook: Tools for Seismic Analysis in Porous Media. Cambridge University Press, Cambridge.

Sayers, C.M., 1994. The elastic anisotropy of shales. J. Geophys. Res., 99: 767-774. doi: 10.1029/93JB02579

Sayers, C.M., 2013. The effect of kerogen on the elastic anisotropy of organic-rich shales. Geophysics, 78(2): D65-D74. doi: 10.1190/geo2012-0309.1

Schoenberg, M. and Protazio, J., 1992. 'Zoeppritz' rationalized and generalized to anisotropy. J. Seismic Explor., 1: 125-144. doi: 10.1121/1.2029011

Vernik, L. and Liu, X. 1997. Velocity anisotropy in shales: A petrophysical study. Geophysics, 62(2), 521-532. doi: 10.1190/1.1444162

Vernik, L. and Nur, A., 1992. Ultrasonic velocity and anisotropy of hydrocarbon source rocks. Geophysics, 57: 727-735. doi: 10.1190/1.1443286

Vernik, L. and Landis, C., 1996. Elastic anisotropy of source rocks: Implications for hydrocarbon generation and primary migration. AAPG Bull. 80(4): 531-544.

Xu, S. and Payne, M.A., 2009. Modeling elastic properties in carbonate rocks. The Leading Edge, 28: 66-74.

Yenugu, M., 2015. Geophysical and geomechanical rock property templates for source rocks. Expanded Abstr., 85th Ann. Internat. SEG Mtg., New Orleans: 3176-3180.

Zeszotarski, J.C., Chromik, R.R., Vinci, R.P., Messmer, M.C.,Michels, R., and Larsen, J.W., 2004. Imaging and mechanical property measurements of kerogen via nano indentation. Geochim. Cosmochim. Acta, 68(20): 4113-4119. doi: 10.1016/j.gca.2003.11.031